Investigation of Ln3+ complexation by a DOTA derivative substituted by an imidazothiadiazole: synthesis, solution structure, luminescence and relaxation properties

Emma Caillet, Léa Nunes, Svetlana Eliseeva, Modou Ndiaye, Manon Isaac, Agnès Pallier, Jean-François Morfin, Hervé Meudal, Stéphane Petoud, Sylvain Routier, et al.

▶ **To cite this version:**

Emma Caillet, Léa Nunes, Svetlana Eliseeva, Modou Ndiaye, Manon Isaac, et al.. Investigation of Ln3+ complexation by a DOTA derivative substituted by an imidazothiadiazole: synthesis, solution structure, luminescence and relaxation properties. Dalton Transactions, 2024, 53 (21), pp.9028-9041. 10.1039/d4dt00533c . hal-04634319

HAL Id: hal-04634319
https://hal.science/hal-04634319v1

Submitted on 12 Nov 2024

HAL is a multi-disciplinary open access archive for the deposit and dissemination of scientific research documents, whether they are published or not. The documents may come from teaching and research institutions in France or abroad, or from public or private research centers.

L'archive ouverte pluridisciplinaire **HAL**, est destinée au dépôt et à la diffusion de documents scientifiques de niveau recherche, publiés ou non, émanant des établissements d'enseignement et de recherche français ou étrangers, des laboratoires publics ou privés.

ARTICLE

Received 00th January 20xx,

Accepted 00th January 20xx

DOI: 10.1039/x0xx00000x

Investigation of Ln^{3+} complexation by a DOTA derivative substituted by an imidazothiadiazole: synthesis, solution structure, luminescence and relaxation properties

Emma Caillet,[a,b] Léa Nunes,[a,b] Svetlana V. Eliseeva,[a] Modou Ndiaye,[a,b] Manon Isaac,[a] Agnès Pallier,[a] Jean-François Morfin,[a] Hervé Meudal,[a] Stéphane Petoud,[a] Sylvain Routier,[b] Carlos Platas-Iglesias,[c] Frédéric Buron *[b] and Célia Bonnet *[a]

We investigated the coordination properties of original macrocyclic Ln^{3+} complexes comprising an imidazothiadiazole heterocycle. The thermodynamic stability of the Gd^{3+} complex was determined by a combination of potentiometric and photophysical measurements. The kinetic inertness was assessed in highly acidic media. The solution structure of the Ln^{3+} complex was unambiguously determined by a set of photophysical measurements and ^{1}H, ^{13}C, ^{89}Y NMR data in combination with DFT calculations, which proved the coordination of the heterocycle to the Ln^{3+}. The ability of the imidazothiadiazole moiety to sensitize Tb^{3+} luminescence was investigated. Finally, the relaxation properties were investigated by recording ^{1}H nuclear magnetic relaxation dispersion (NMRD) profiles and ^{17}O measurements. The water exchange rate is similar to that of GdDOTA as the less negative charge of the ligand is compensated by the presence of a bulky heterocycle. The relaxivity is constant over a large range of pH, demonstrating the favorable properties of the complex for imaging purposes.

Introduction

Lanthanide ions (Ln^{3+}) are widely used for a broad range of applications ranging from biomedical applications, telecommunications, catalysis or metallurgy, to cite a few.[1] Their unique magnetic and optical properties, combined with a similarities in chemical properties, makes them unique in the periodic table.[2] In the last decades, coordination compounds formed with Ln^{3+} have attracted much attention due to their successful biomedical applications, both in diagnosis and therapy.[3-10] For example, several Gd^{3+} complexes have been clinically-approved as Magnetic Resonance Imaging (MRI) contrast agents.[3] Furthermore, several paramagnetic Ln^{3+} are luminescent and can be used for optical imaging or as probes in bioassays.[11] Ln^{3+} complexes used in biological applications need to be sufficiently water soluble and display a high thermodynamic stability and kinetic inertness. Moreover, if they are to be used for their photophysical properties, a chromophore, suitable to transfer energy to the accepting electronic levels of Ln^{3+} ion, must be present in sufficient close proximity to ensure an antenna effect. Macrocyclic derivatives based on DOTA (1,4,7,10-tetraazacyclododecane-1,4,7,10-tetraacetic acid) are widely used for Ln^{3+} complexation due to their high thermodynamic stability and exceptional kinetic inertness.[12] DO3A derivatives, for which one acetate arm is absent, have been widely studied as they can be easily functionalized to attach a chromophore,[11, 13] a chemically[14-16] or biologically[17-19] active group.

Heterocycles are versatile moieties as they can potentially coordinate directly to the Ln^{3+} ion and be used as chromophores or as scaffolds for bioactive molecules. However, the direct coordination of the Ln^{3+} ion to the heterocycle has been underexplored, and mainly restricted to the use of pyridine derivatives[20-23], or strictly as chromophore for Ln^{3+} luminescence sensitisation.[24]

Among the variety of heterocyclic compounds, imidazole or thiadiazole are widely used in coordination chemistry, in particular for the formation of organometallic frameworks and functional materials.[25, 26] These two cycles can be combined together in a [5-5] fused ring with a bridgehead nitrogen atom, affording imidazo[2,1-*b*][1,3,4]thiadiazoles. This bicyclic structure exhibits various biological activities[27] such as antifungal, anticancer, antihyperlipidemic, antimicrobial, anti-inflammatory, antituberculosis, anticonvulsant, analgesic, and diuretic properties.[27-36] Therefore, imidazo[2,1-*b*][1,3,4]thiadiazole and their derivatives have become important structures used in pharmaceutical chemistry.[37-42] The combination of the coordinating properties and biological potential of imidazothiazoles are appealing to generate original Ln^{3+} complexes.

In this context, we have recently synthesized L1 and L2 (Scheme 1), which contain an imidazo[2,1-*b*][1,3,4]thiadiazole

[a] *Centre de Biophysique Moléculaire CNRS UPR 4301, Université d'Orléans, Rue Charles Sadron, 45071 Orléans Cedex 2, France.*
[b] *Institut de Chimie Organique et Analytique UMR CNRS 7311, Université d'Orléans, Rue de Chartres, BP6759, 45067 Orléans Cedex 2, France.*
[c] *Universidade da Coruña, Centro de Interdisciplinar de Química e Bioloxía (CICA) and Departamento de Química, Facultade de Ciencias, 15071, A Coruña, Galicia, Spain.*

† Footnotes relating to the title and/or authors should appear here.
Electronic Supplementary Information (ESI) available: [details of any supplementary information available should be included here]. See DOI: 10.1039/x0xx00000x

Please do not adjust margins

heterocycle, linked to a DO3A monoamide macrocycle, and studied the corresponding Ln^{3+} complexes.[43] The heterocycles sensitize the Tb^{3+} luminescence with relatively modest quantum yield values, and the corresponding Gd^{3+} complexes show optimised relaxivities compared to the GdDOTA gold standard. In these systems the heterocycle is linked to the macrocycle through an amide function and does not participate to the coordination sphere of the Ln^{3+}.

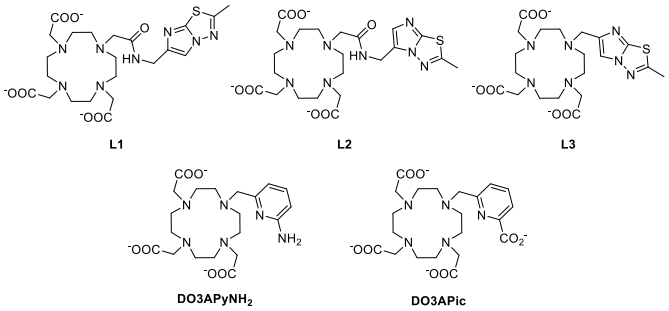

Scheme 1. Structure of the ligands discussed in this work.

Here, we describe the synthesis of L3 (Scheme 1), in which the heterocycle is directly attached to the macrocycle. To the best of our knowledge, this is the first time that such bioactive scaffold is directly linked to a macrocycle for Ln^{3+} complexation. This should impact the luminescence properties of the Tb^{3+} complex, but also the relaxation properties through the modification of the Ln^{3+} coordination sphere. To explore the potential of those compounds, it is of prime importance to determine the thermodynamic stability and kinetic inertness of the Ln^{3+} complexes, as well as to probe their structure in solution. The protonation constants of the ligand and the thermodynamic stability of the Gd^{3+} complex were determined by pH-potentiometric titrations combined with UV-visible spectroscopy. The kinetic inertness of the Gd^{3+} complex was evaluated in acidic media. The solution structure of the Ln^{3+} complex was determined using ^{1}H, ^{13}C, and ^{89}Y NMR, combined with DFT calculations. The luminescent properties of the Tb^{3+} complex were investigated and the number of water molecules directly coordinated to the Tb^{3+} ion was determined. Finally, the relaxation properties of the Gd^{3+} complex were investigated by relaxometry and ^{17}O NMR to access the exchange rate of the inner-sphere water molecule.

Results and discussion

Synthesis of the Ligand L3

The chlorine derivative **4**, which can be prepared in three steps from commercially available 2-amino-5-methyl-1,3,4-thiadiazole **1,** is a key compound in the synthesis of L3. The condensation of **1** and ethyl bromopyruvate in ethanol under microwave activation led to the formation of the ester **2** in moderate yield (30%). In the next step, the ester **2** was reduced with DIBAL-H at room temperature in DCM to generate the primary alcohol **3** in 89% yield. The chlorination of the alcohol with thionyl chloride led to derivative **4** with a 59% yield. Finally, ligand L3 was obtained in two steps. The *N*-alkylation of DO3AtBu was performed in the presence of chlorinated derivative **4** and K_2CO_3 as base in acetonitrile at 60°C during 3h, followed by the cleavage of *t*-Butyl esters with a HCl 10 M solution in dioxane at 50°C during 16h**. L3** was isolated in 25% yield over two steps. The ^{1}H and ^{13}C NMR spectra of the various compound are presented Figures S1-4 (ESI†).

Scheme 2. Synthetic pathway to access L3

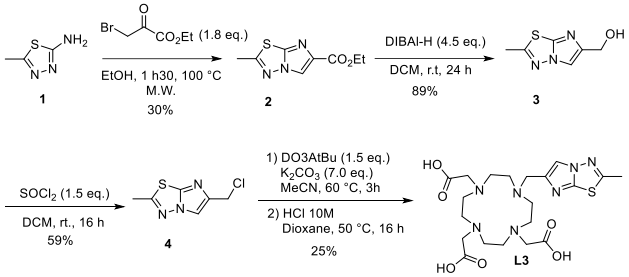

Protonation constants of the ligand L3 and stability of the complexes

Potentiometric studies of L3 were performed in order to determine the species present in solution through the evaluation of their equilibrium constants. The ligand protonation constants were assessed, as defined in equation 1.

$$\boldsymbol{K_i} = \frac{[\boldsymbol{H_iL}]}{[\boldsymbol{H_{i-1}L}][\boldsymbol{H}]} \quad (1)$$

L3 displays seven protonation constants (Table 1). By comparison with L2,[43] the first three protonation constants can be attributed to one nitrogen of the heterocycle and two amine groups of the macrocycle. The other protonation constants can be attributed to another nitrogen of the heterocycle, carboxylate functions and/or the remaining nitrogen from the macrocycle. In order to attribute more precisely those protonation constants, UV absorption, excitation and emission spectra of L3 were recorded in the pH range 2-12 (Figure 1 and S5-6, ESI†). Upon excitation at 300 nm, an emission band with a maximum at 410 nm is observed. The intensity decreases with decreasing pH. By fixing the emission at 400nm, the excitation spectra show a maximum at 295 nm, which also decreases with decreasing pH. The UV-absorption, emission and excitation spectra as a function of pH were fitted to obtain the protonation constants of the system. The results, presented in Table 2, show the presence of two protonation constants for the heterocycle. These protonation constants are in the same range than those previously found for L1 and L2.[43] They also match very well the values of Log K_{H1} and Log K_{H5} found by potentiometry. The first protonation constant of the macrocycle (9.25) is slightly lower than that of DOTA, certainly due to the electron-withdrawing effect of the heterocycle. Indeed, it matches well the values obtained for DO3Apic[44] and $DO3APyNH_2$.[45]

 This journal is © The Royal Society of Chemistry 2024

Please do not adjust margins

Table 1: Protonation constants measured in NaCl (0.15 M) at 298 K.

Log K_H	L3	L2[a]	DO3APyNH$_2$[b]	DO3APic[c]	DOTA[d]
Log K_{H1}	9.4 (1)	9.09	9.12	9.21	9.37
Log K_{H2}	9.25 (6)	8.98	9.29	8.94	9.14
Log K_{H3}	9.24 (3)	8.51	7.71	4.82	4.63
Log K_{H4}	4.90 (4)	4.77	4.26	3.52	3.91
Log K_{H5}	4.10 (8)	3.97	2.11	1.39	
Log K_{H6}	3.62 (9)	3.76			
Log K_{H7}	1.57 (3)	2.33			
Log K_{H8}		2.1			

[a] From ref. [43]. [b] From ref.[46] [c] From ref.[44] [d] From ref.[47], in 0.1 M NaCl.

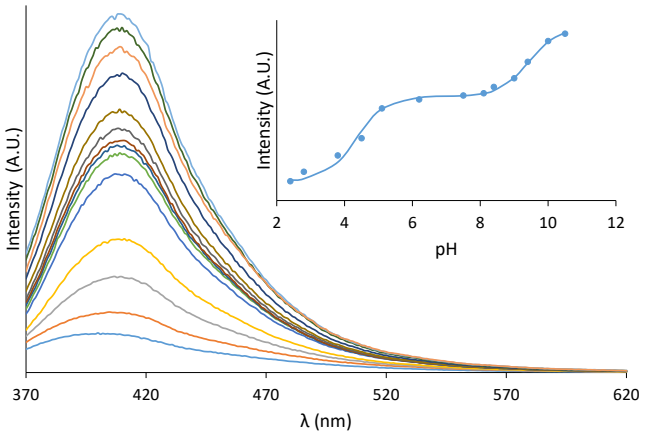

Figure 1: Normalized emission spectra (λ_{exc} = 300 nm) of L3 (150 µM) in 0.15 M NaCl at 298 K; Inset: Emission intensities at 400 nm as a function of pH. The line represents the best fit of the data affording the values given Table 2.

Complex stability and protonation constants, logK_{ML}, logK_{MLH} and LogK_{MLOH} (equations 2, 3 and 4) have been determined for Gd^{3+} as well as for Zn^{2+} and Ca^{2+} (Fig. 2 and S7, ESI†).

$$K_{MmL} = \frac{[M_mL]}{[M_{m-1}L][M]} \quad (2)$$

$$K_{MmLHi} = \frac{[M_mL]}{[M_mLH_{i-1}][H]} \quad (3)$$

$$K_{MLOH} = \frac{[ML]}{[ML(OH)][H]} \quad (4)$$

Table 2: Protonation constants of L3 and GdL3 determined by UV and fluorescence titrations in 0.15 M NaCl at 298 K

		UV	Emission	Excitation
L3	Log K_{H1}	9.6 (1)	9.4 (1)	9.0 (2)
	Log K_{H2}	4.1 (1)	4.3 (1)	4.40 (8)
GdL3	Log K_{H1}	nd[a]	9.4 (1)	9.1 (2)
	Log K_{H2}	nd[a]	3.8 (1)	4.3 (1)

[a] Not determined

Due to the slow formation kinetics of the complex, Gd^{3+} stability constants were determined by the out-of-cell batch method, while those for Zn^{2+} and Ca^{2+} could be obtained with an automated titration (Figure 2 and S7, ESI†). The different species formed and their stability constants are summarised in Table 3. The stability constant found for GdL3 is lower than that of GdDOTA but in the same order of magnitude than that of the eight-coordinated GdPyNH$_2$.[46] Surprisingly, GdL3 shows two protonation constants of 9.0 and 4.5. The species distribution in a 1/1 molar ratio (Figure S8, ESI†) indicates that the major species present at physiological pH is GdLH. The absorption spectra of GdL3 as a function of pH do not show important changes (see Figure S9, ESI†), suggesting that the heterocycle has different features in the complex than in the free ligand. However, emission and excitation spectra of GdL3 vary significantly as a function of pH (Figure S10-11, ESI†), and the fit of those data gives protonation constants consistent with the potentiometric data (Table 2). Two nitrogen atoms can be protonated on the heterocycle, and the first protonation constant most certainly corresponds to the protonation of the nitrogen from the thiazole moiety. The protonation constant at 4.5 could be attributed to the protonation of the nitrogen from the imidazole moiety. However, it cannot be excluded that it belongs to a carboxylate function as similar protonations have been evidenced by X-ray structures on a few examples of DOTA-like complexes.[48-50] The presence of the neighbouring heterocycle could stabilize this protonation through hydrogen bond explaining both a higher than expected value for the protonation of carboxylate functions, and the modification of the UV and fluorescence properties of the complex.

Table 3: Stability constants of the different complexes measured by potentiometric titration in NaCl (0.15 M) at 298 K.

Log K	L3	DO3APyNH$_2$ [a]	DO3APic	DO3A [d]	DOTA
GdL	18.1(2)	18.60	23.31[b]	19.06	24.7[e]
GdLH	9.0(1)	3.92	2.65		
GdLH$_2$	4.5(1)				
GdLOH	11.6(1)				
ZnL	18.8(1)	16.71	20.25[c]	21.57	20.21[d]
ZnLH	9.27(3)	6.61	4.42	3.47	
ZnLH$_2$	4.4(4)	3.98	3.06	2.07	
ZnLH$_3$	3.84(3)	2.96	1.98		
ZnLH$_4$	2.95(4)				
CaL	13.56(3)	11.88	14.82[c]	12.57	16.11[d]
CaLH	9.32(2)	5.38	4.59	4.60	
CaLH$_2$	4.14(6)		4.32		
pGd[f]	15.0	15.5	20.96		19.2

[a] From ref. [45] [b] From ref.[44] [c] In 0.1 M KCl; from ref.[51] [d] From ref. [52] [e] In 0.1 M NaCl; from ref. [47] [f] pGd = -Log[Gd]$_{free}$ at pH 7.4 with [Gd] = 1.10^{-6} M and [L] = 1.10^{-5} M

In order to assess the selectivity of L3 for Ln^{3+} versus other important physiological cations, potentiometric titrations were also performed with Zn^{2+} and Ca^{2+}.The stability constant value of ZnL3 is slightly higher than that of GdL3, and interestingly two orders of magnitude higher than that of ZnPyNH$_2$, suggesting an important role of the heterocycle in Zn^{2+} coordination. The lack of selectivity for Gd^{3+} vs Zn^{2+} is compensated by the high kinetic inertness of the system (*vide infra*). ZnL3 shows two

Please do not adjust margins

protonation constants, in the same range as those of GdL3. The presence of the second protonation constant certainly explains the relatively high stability constant of the Zn^{2+} complex compared to Gd^{3+}. Finally, CaL3 behaves similarly as ZnL3, with a higher stability constant than CaPyNH2, and two protonation constants.

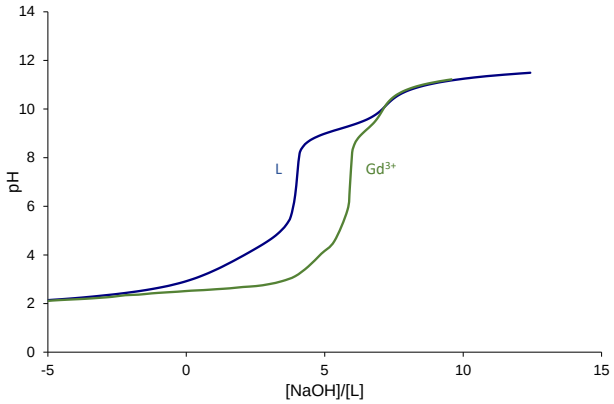

Figure 2: Potentiometric titration curves of solutions containing L3 (1.3 mM) with 0 or 1 equivalents of $GdCl_3$ in 0.15 M NaCl, 298 K.

Kinetic inertness

Kinetic inertness is also an important parameter to assess the toxicity of a given complex. Due to their preorganized structure, macrocyclic ligands are known to form complexes with high kinetic inertness compared to acyclic ligands. Dissociation can occur via the metal-assisted pathway, using physiological cations such as Zn^{2+} or Cu^{2+}, or proton-assisted pathways. Metal-assisted dissociation pathways are very often triggered by the formation of dinuclear complexes. In the case of DOTA derivatives, such formation is not commonly observed, leading to very slow dissociation. However, in this case, the stability constant of the Zn^{2+} complex is in the same order of magnitude than that of the Gd^{3+} complex. We therefore decided to investigate the Zn^{2+}-catalysed dissociation of GdL3. This reaction was followed by monitoring the increase in the longitudinal proton relaxation rate at pH 5, and 2 in the presence of 10 eq. or 20 eq. of Zn^{2+} (Figure S12, ESI†). No significant increase in the relaxation rate was observed after a week at pH 2, and a month at pH 5. This means that the metal-assisted pathway is certainly negligible. This also means that the Zn^{2+} cannot replace Gd^{3+} within the macrocycle despite the higher stability constant of ZnL3 vs GdL3, due to the good kinetic inertness of the system. In order to explore the proton-assisted pathway, we used Eu^{3+} as an exchanging ion to accelerate the dissociation. We followed the dissociation as previously in the presence of 10 eq. of Eu^{3+} at pH 2, 3 and 5.5 (Figure S13, ESI†). After more than one week, even at pH 2 (where thermodynamically the complex is not stable) no significant dissociation was observed.

Therefore, in order to characterize the kinetic inertness of GdL3 and compare it with those of other complexes, we decided to follow the dissociation in highly acidic conditions (1 M HCl). Under these conditions, the complex is not stable and dissociates completely. Given the very high H^+ concentration, the dissociation follows a pseudo-first order of kinetics and the dissociation rate is directly proportional to the total concentration of the complex $[LnL]_t$ (corresponding to the sum of the concentration of protonated and non-protonated complexes), where k_{obs} is the observed pseudo-first order rate constant:

$$-\frac{d[LnL]_t}{dt} = k_{obs}[LnL]_t \quad (6)$$

Table 4: Rate constants characterizing the complexes dissociation determined in 1 M HCl (0.15 M NaCl, unless otherwise stated) at 298 K, and half-life in the same conditions

	k_{obs} (s^{-1})	$t_{1/2}$ (min)
GdL3	$1.8.10^{-4}$	64
GdDOTA [a]	$1.8.10^{-6}$	6418
GdDO3A [b]	$2.3.10^{-2}$	0.5
EuDO3Apic[c]	$2.0.10^{-3}$	5.7
GdDO3APyNH$_2$[d]	$9.1.10^{-2}$	0.13

[a] From ref [53]. [b] In 0.1 M KCl from ref [54]; [c] In 0.1 M KCl from ref [44] [d] From ref. [46]

The k_{obs} value determined for GdL3 is presented in Table 4, together with the calculated dissociation half-life in 1 M HCl. The kinetic inertness of GdL3 is lower than that of GdDOTA, but much higher than that of the seven coordinate GdDO3A (k_{obs} two orders of magnitude higher). Interestingly, the k_{obs} value of GdL3 is one order of magnitude lower than that of $GdDO3APyNH_2$ and EuDO3APic. The lower kinetic inertness of $GdDO3APyNH_2$ was explained by the presence of a protonable amine function (log K_{GdLH} = 3.92), which largely accelerates the proton assisted dissociation.[46] In the case of GdL3, two protonation constants are observed (log K_{GdLH} = 9.0 and log K_{GdLH2} = 4.5). The first one corresponds to the protonation of the nitrogen atom from the thiazole core, which is far away from Gd^{3+} explaining the low impact in complex dissociation. However, the second protonation constant, from the nitrogen of the imidazole moiety or a neighbouring carboxylate function, is in close proximity with the Gd^{3+} centre, and can accelerate the dissociation. For EuDO3APic, the carboxylate function of the picolinate group coordinates at a sterically demanding capping position, and thus protonation of the picolinate moiety facilitates complex dissociation.[55, 56]

Structural study of the complex

In order to determine the structure of the LnLH complex at physiological pH, we performed NMR studies on various Ln^{3+} complexes. First, we recorded the ^1H NMR spectrum of EuL3H at 700 MHz, 298 K (Figure S14, ESI†). The spectrum shows two sets of 26 signals, which is indicative of a C_1 symmetry and the presence of two isomers. It is well-known that in nine-coordinate Ln^{3+} DOTA-like complexes, there are two possible conformations of the macrocycle, (δδδδ) and (λλλλ), dictated by the gauche conformations of the individual ethylenediamine groups. Moreover, the four pendant arms can have two possible orientations (absolute configuration Δ and Λ). All this results in four possible isomers, existing as two enantiomeric pairs. These isomers adopt either a monocapped square antiprismatic (SAP) or a monocapped twisted square

 This journal is © The Royal Society of Chemistry 2024

Please do not adjust margins

Please do not adjust margins

antiprismatic (TSAP) geometry.[57, 58] The chemical shifts of the axial ring protons of the major isomer (29.75, 29.17, 28.59, 27.68 ppm) and minor isomer (11.16, 10.97, 9.42, 9.24 ppm) isomer are similar to those described for the SAP and TSAP isomers of EuDOTA derivatives, respectively.[54, 59] Therefore, by comparison of the two sets of signals (Figure S15, ESI†), it is estimated that 60 % of EuL3H exists as the SAP isomer and 40 % as the TSAP isomer under these experimental conditions. At the same temperature, the populations of the two isomers in EuDOTA are ca. 80:20 (SAP:TSAP),[59] indicating that the presence of the heterocyclic arm stabilises slightly the TSAP isomer. This is in line with previous studies, which indicated that an increasing steric hindrance favours the TSAP isomer.[60]

The fact that the EuL3H complex provides a well-resolved ^{1}H NMR spectrum suggests coordination of the heterocyclic arm to the metal ion, as EuDO3A derivatives generally show broad signals in their NMR spectra due to their fluxional behaviour. This is due to a low activation barrier for the arm rotation pathway responsible for the SAP↔TSAP exchange process. On the contrary, complexes in which four pendant arms are involved in coordination display rather high activation energies for both the rotation of the pendant arms and the (δδδδ) ↔ (λλλλ) inversion of the cyclen unit. The presence of a single water molecule coordinated to the metal centre, evidenced by both luminescence and relaxometric studies (vide infra), is also in line with the coordination of the heterocycle, as GdDO3A derivatives contain two water molecules coordinated to the metal ion. However, we cannot exclude a 8-coordinated Ln^{3+} complex due to the steric hindrance of the heterocycle. Thus, we performed a DFT study to gain additional insight on the structure of the complex in solution. For this purpose, we modelled the SAP isomer of the GdL3H complex incorporating up to six water molecules. The incorporation of a few explicit second-sphere water molecules is required for a better description of the bond distances involving inner-sphere water molecules and the number of water molecules directly coordinated to the metal ion. Calculations performed on the GdL3H·6H_2O system using the wB97XD functional provide three SAP energy minima, one with the heterocycle coordinated to the metal ion and a coordinated water molecule (Figure 3), a second geometry with the arm uncoordinated and two coordinated water molecules, and a third energy minimum with the uncoordinated heterocycle and one inner-sphere water molecule. (Figure 3). Our calculations indicate that the geometry in which the heterocycle is coordinated (N_5O_4 donor set) is much more stable compared those lacking heterocycle coordination, either having one (N_4O_4 donor set, ΔG = +9.6 kcal mol^{-1}, Figure S18, ESI†) or two coordinated water molecules (N_4O_5 donor set, ΔG = +11.78 kcal mol^{-1}, Figure S19, ESI†). This excludes the possibility of a stable 8-coordinated Ln^{3+} within the complex.

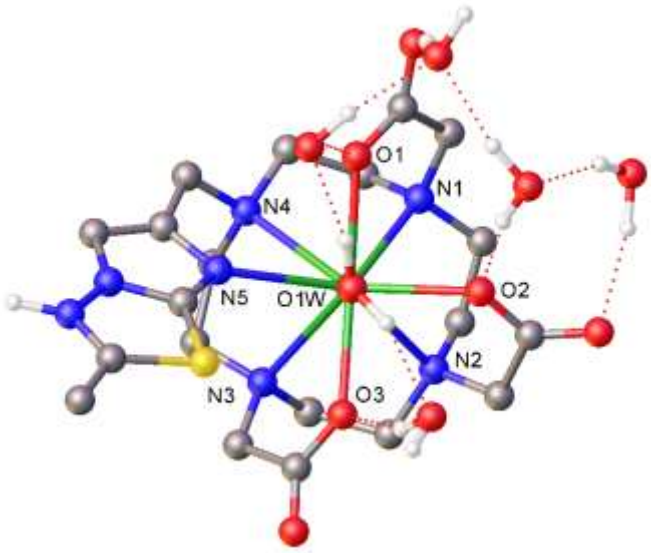

Figure 3: Geometry of the GdL3H·6H2O system optimized using DFT calculations (wB97XD functional). Hydrogen atoms bonded to C atoms are omitted for simplicity. Bond distances of the Gd(III) coordination environment (Å): Gd-N1, 2.697; Gd-N2, 2.674; Gd-N3, 2.713; Gd-N4, 2.783; Gd-N5, 2.549; Gd-O1, 2.387; Gd-O2, 2.352; Gd-O3, 2.384; Gd-O1w, 2.500.

The diamagnetic Y^{3+} complex was also synthesized and its ^{1}H NMR spectrum was recorded in D_2O (Figure S16, ESI†). The assignment of the proton signals (Table S1, ESI†) were based on standard 2D experiments (COSY, HSQC, HMBC). Interestingly, the CH_2 between the macrocycle and the heterocycle shows two resonances with a strong geminal coupling, which is characteristic of the absence of free rotation of this CH_2. This is consistent with the two signals observed for this same CH_2 in the corresponding Eu^{3+} complex, confirming heterocycle coordination.

^{89}Y NMR shifts are also very informative on the metal environment.[61] The chemical shift of ^{89}Y can be obtained using ^{1}H,^{89}Y heteronuclear shift correlation through scalar coupling (HMQC). As the relaxation time of ^{89}Y is very long (200-500 s), this allows a much faster acquisition. The spectrum of YL3H, which is presented Figure 4, shows clear cross-peaks correlating the ^{89}Y NMR signal and the equatorial protons of the pendant arms situated three bonds away the metal ion (H5, H8, H11 and H14) The ^{89}Y NMR chemical shift obtained from this experiment (120.20 ppm) is very similar to those reported for DOTA-tetraamide derivatives including $[Y(DOTAM)]^{3+}$.[61] Furthermore, the ^{89}Y NMR signal is significantly more shielded in [Y(DO3A)] (103 ppm)[61] than in YL3H, which we attribute to the coordination of the heterocyclic unit in the latter.

Please do not adjust margins

Please do not adjust margins

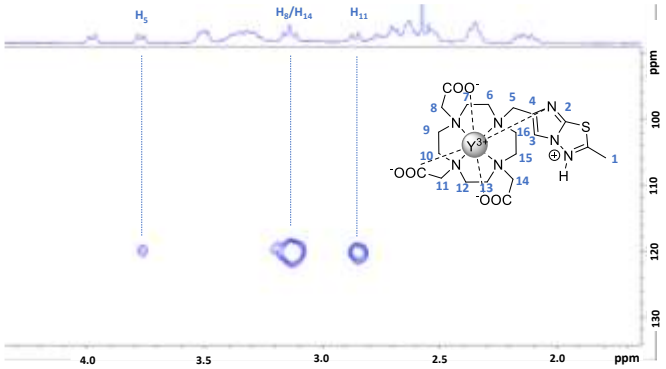

Figure 4: $^{1}H,^{89}Y$-HMQC spectrum of YL3H recorded in D_2O, 4.60 mM, pD 7.36.

The ^{89}Y NMR chemical shift can be approximated by an empirical expression that adds the contributions of the individual donor atoms:[61]

$$\delta^{calc}(^{89}Y) = 863 - (4\ S_{Nam} + S_{Ow} + 3\ S_{Oc} + S_{Nhet}) \quad (7)$$

Taking the tabulated values for the shielding constant amine groups (S_{Nam} = 68.1 ppm), carboxylate oxygen atoms (S_{Oc} = 94.0 ppm) and coordinated water molecules (S_{Ow} = 107.6 ppm), and estimating the contribution of the heterocycle (S_{Nhet}) from that reported for pyridine *N* atoms (S_{Npy} = 85.7 ppm), we obtain $\delta^{calc}(^{89}Y)$ = 115.3 ppm. The good agreement between the experimental shift and that obtained with the aid of the empirical correlation confirms heterocyclic binding and the presence of a water molecule coordinated to the metal ion.

Table 5: Isotropic ^{89}Y NMR shielding constants (σ_{iso}), their paramagnetic (σ_{para}) and diamagnetic (σ_{dia}) contributions, and chemical shifts obtained with relativistic DFT calculations.[a]

	Donor set	σ_{iso}	σ_{dia}	σ_{para}	δ_{calc}
YL3**H**·6H_2O	N_5O_4	2554.1	3627.3	-1073.2	122.4
YL3**H**·6H_2O	N_4O_5	2573.7	3626.2	-1052.5	102.8
YL3**H**·6H_2O	N_4O_4	2524.7	3627.6	-1102.8	151.8
[Y(H_2O)$_8$]$^{3+}$	O_8	2676.5	3617.0	-940.5	0.0
[a] All data in ppm.					

The ^{89}Y NMR chemical shifts were also calculated using relativistic DFT, to provide support to the analysis performed using the predictions of Eq (7). For this purpose, we optimized the geometries of the YL3H·6H_2O system and calculated the ^{89}Y NMR shielding tensors using the TPSSh functional, which was found to provide good results for this problem. These calculations yielded the shielding constants shown in Table 5, as well as the corresponding diamagnetic and paramagnetic contributions.[62] For chemical shift calculation purposes, we also calculated the shielding constants for the $[Y(H_2O)_8]^{3+}$·16H_2O system. DFT gives calculated shifts in excellent agreement with the experiment when using the model structure with the heterocyclic arm involved in the Ln^{3+} coordination (N_5O_4 donor set). The model structure that contains two inner-sphere water molecules and an uncoordinated heterocyclic unit (N_4O_5 donor set) deviates by 19.5 ppm from the experimental data. Furthermore, the structure with an uncoordinated heterocycle and only one coordinated water molecule (N_4O_4 donor set) deviates even further from the experimental data up to ~30 ppm. Thus, our DFT calculations confirm that the complex exists in solution as a mono-hydrated species in which all four pendant arms are coordinated to the metal ion.

These calculations give very similar diamagnetic contributions to the isotropic shielding constant σ. This is expected, as the diamagnetic contribution arises from changes in the local magnetic field at the ^{89}Y nucleus associated to the charge distribution. The paramagnetic contributions involve contributions from excited states, and it is the main factor affecting the chemical shifts.

Photophysical properties

Photophysical properties were studied for 0.5 mM solution of TbL3H in HEPES buffer (pH = 7.4). The absorption spectrum presents broad bands in the UV range up to 300 nm (Figure 5). The excitation spectrum collected upon monitoring the Tb^{3+} emission at 543 nm is dominated by broad ligand-centred bands in the UV range (Figure 6, top) reflecting the ability of the imidazothiadiazole-based chromophore to sensitize the visible luminescence of Tb^{3+} through the 'antenna effect'.[63] In addition, in the excitation spectrum, sharper features corresponding to Tb^{3+} f-f transitions are present in the UV and visible ranges indicating the direct excitation of the Tb^{3+} metal ion in TbL3H. Upon excitation into the ligand-centred bands at 270 nm, TbL3H exhibits green emission with sharp features in the range of 480–700 nm due to the $^5D_4 \rightarrow {}^7F_J$ (J = 6–0) transitions of Tb^{3+} in addition to broader ligand-centred bands located in the range 300–450 nm (Figure 6, bottom). The measured Tb^{3+}-centred quantum yield (Q_{Tb}^{L}) value was found to be (0.21±0.02) %. This relatively small value can be partially explained by the low efficiency of this chromophore to operate as a sensitizer of Tb^{3+} emission. Nevertheless, the value of Q_{Tb}^{L}. of TbL3H is 10-13 times higher than the ones reported for comparable Tb^{3+} complexes formed with imidazothiadiazole-based chromophores, which can be explained by the direct coordination of the heterocycle to the Tb^{3+}.[43] In order to estimate the number of water molecules coordinated to Tb^{3+} (q) using phenomenological equations described in the literature,[64] luminescence decays were recorded for solutions of TbL3H in HEPES buffer (pH = 7.4) and D_2O (pD = 7.4). It was found that the experimental decay curves are best fitted with bi-exponential functions (Table S2, ESI†), indicating the presence of Tb^{3+} cations present in different coordination environments or differently affected by non-radiative quenching processes. Average Tb^{3+} luminescence lifetimes were calculated to be (1.5±0.02) ms and (2.4±0.01) ms for solutions in HEPES buffer and D_2O, respectively, giving the value of q equal 1.1, supporting previous DFT calculations.

 This journal is © The Royal Society of Chemistry 2024

Please do not adjust margins

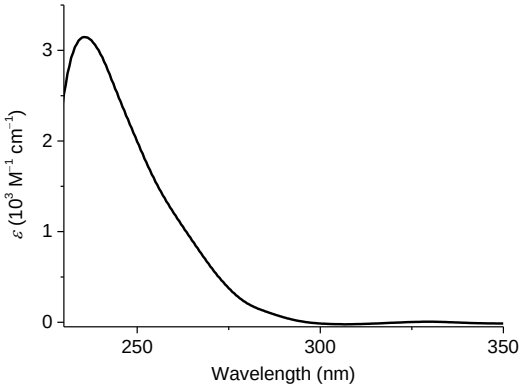

Figure 5. Absorption spectrum of TbL3H (0.5 mM, HEPES pH 7.4, room temperature).

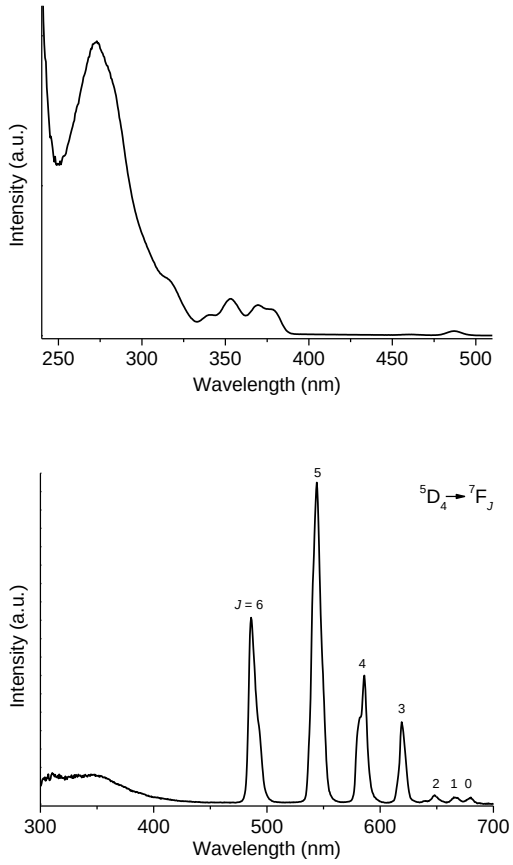

Figure 6. Corrected and normalized (top) excitation spectrum collected upon monitoring the Tb^{3+} emission at 543 nm and (bottom) emission spectrum upon excitation at 270 nm of 0.5 mM solution of TbL3H in HEPES buffer (pH 7.4, room temperature).

Relaxation properties

To determine the relaxivity of the Gd^{3+} complex, Paramagnetic Relaxation Enhancements (PRE) were measured at 60 MHz and 25°C as a function of concentration (Figure S20, ESI†). The PREs are linear with the concentration indicating the absence of aggregation process in the concentration range studied. The relaxivity was found to be 4.11 $mM^{-1}.s^{-1}$ at 20MHz, 25°C, that is, slightly lower than that of GdL1 and GdL2 (4.58 and 4.50 $mM^{-1}.s^{-1}$, respectively), and higher than that of GdDOTA (r_1 = 3.70 $mM^{-1}.s^{-1}$).

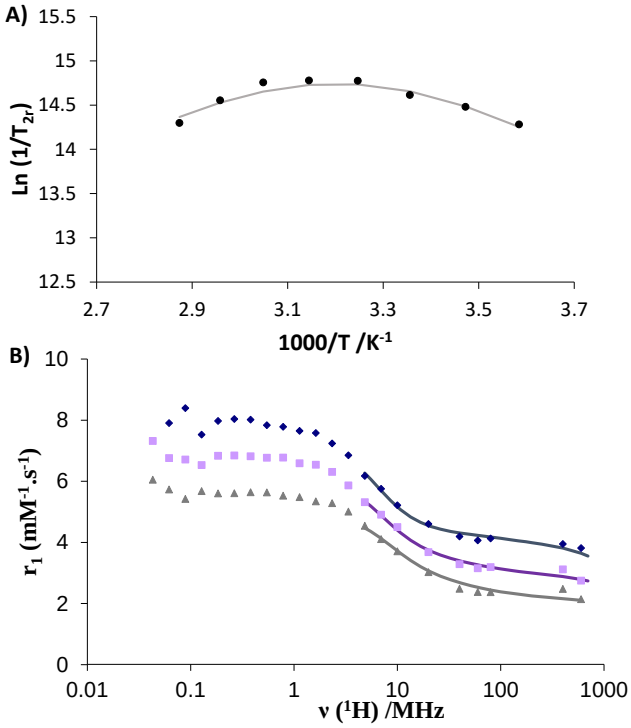

Figure 7: A) Temperature dependence of the reduced ^{17}O transverse relaxation rates (top) of GdL3H (1.8 mM) at 9.4 T. B) NMRD profiles of GdL3H (1.09 mM) at 25°c (blue ♦), 37°C (purple ■), and 50°C (grey ▲). The curves represent the simultaneous fit to the experimental data points.

To characterise the parameters governing proton relaxivity of the complex, nuclear magnetic relaxation dispersion (NMRD) profiles were recorded at three different temperatures (Figure 7B). Since the relaxivity is determined by several physicochemical parameters, including water exchange rate, electron relaxation parameters and rotational correlation times, it is important to assess the maximum of these parameters independently. In the case of GdL3H, the relaxivity is decreasing with increasing temperature, which is characteristic of small molecular complex for which relaxivity values are limited by the rotation of the system. The water exchange rate is strongly influenced by the Gd^{3+} coordination sphere (type of coordinating function, steric hindrance, coordination number).[65] The coordination sphere of GdL3H is not classical, therefore it is interesting to determine the water exchange rate of the system independently, even if it does not strongly influence relaxivity values. To do so, ^{17}O NMR spectroscopy has been used.

Variable temperature ^{17}O T_2 measurements give access to the water exchange rate, k_{ex}. It is also possible to obtain information about the rotational correlation time, τ_R, by recording the ^{17}O T_1 data, which is determined by dipole-dipole and quadrupolar relaxation mechanisms. Finally, the ^{17}O

Please do not adjust margins

chemical shifts gives indication of the number of water molecules directly coordinated to Gd^{3+}, *q*. Longitudinal and transverse ^{17}O relaxation rates and chemical shifts were measured as a function of the temperature on aqueous solutions of GdL3H and on a diamagnetic reference. The longitudinal relaxation rates, and chemical shifts measured for GdL3H were too close to those of the reference and were therefore excluded from the analysis. The reduced ^{17}O transverse relaxation rates are presented in Figure 7A. The ^{17}O-reduced transverse relaxation rates first increase (up to *ca.* 310 K), then decrease with increasing temperature. It indicates that the complex is in the slow kinetic region at low temperatures and in the fast exchange region at higher temperatures. In the slow kinetic region, $1/T_{2r}$ is directly determined by the exchange rate constant k_{ex}, whereas in the fast exchange region, it is determined by the transverse relaxation rate of the coordinated water oxygen, $1/T_{2m}$, which is in turn influenced by the water exchange rate, k_{ex}, the longitudinal electronic relaxation rate, $1/T_{1e}$, and the scalar coupling constant, A/ħ. In our case, the slow kinetic region is well-defined and enables a reliable determination of k_{ex}.

The transverse ^{17}O relaxation rates, and the NMRD profiles, were simultaneously analysed with the Solomon-Bloembergen and Morgan (SBM) theory to yield the microscopic parameters characterising water exchange and rotation (see ESI for equations). Indeed, if we are not interested in detailed information about the electron spin relaxation and if we restrict the analysis of the NMRD data to medium and high magnetic fields, the SBM approach gives reliable information on dynamic processes like water exchange and rotational correlation times for small complexes.[66, 67] Therefore we decided to include only relaxivity values above 6 MHz in the fitting process.

In the analysis of the data, several parameters have been fixed to common values. The hydration number was fixed to 1 as the complex was proved to be monohydrated both by luminescence lifetime measurements on the corresponding Tb^{3+} complex, and by DFT calculations. r_{GdO} was fixed to 2.5 Å as shown by DFT calculations (*vide supra*). This is also the distance commonly used for polyaminopolycarboxylate complexes based on available crystal structures and ENDOR results.[68] The quadrupolar coupling constant, $\chi(1+\eta^2/3)^{1/2}$, was set to the value for pure water, 7.58 MHz.[69] The diffusion coefficients D_{GdH}^{298} = 26.10^{-9} m^2.s^{-1} were fixed, and the corresponding activation energies E_{DGdH} were fitted. The Gd-water proton distance was fixed to r_{GdH} = 3.1Å, the closest approach between the Gd^{3+} ion and the outer sphere protons was fixed to a_{GdH} = 3.6 Å, and the scalar coupling constant, *A*/ħ was fixed to -3.6.10^6 rad.s^{-1}. The following parameters have been adjusted: the water exchange rate, k_{ex}^{298}, the activation enthalpy for water exchange, $\Delta H^{\neq}$, the rotational correlation time, τ_R^{298}, and its activation energy, E_R, and the parameters describing electron spin relaxation, the mean square of the zero field splitting, Δ^2, the correlation time for the modulation of the zero field splitting, τ_V^{298}, while its activation energy, E_V has been fixed to 1 kJ/mol. The parameters resulting from the best fit are presented in Table 6 and S4.

Table 6: Parameters obtained from the simultaneous fitting of the transverse ^{17}O NMR relaxation rates as a function of temperature at 9.4 T, and of the NMRD profiles at 298 K, 310 K, and 323 K, using the Solomon Bloembergen and Morgan theory presented in ESI.

	GdL3H	GdL1[a]	GdDO3APyNH$_2$[b]	GdDOTA[c]
r_1 (mM^{-1}.s^{-1}), 60 MHz, 25°C	4.11	4.58	4.04	3.7
k_{ex}^{298} (10^{6}s^{-1})	4.8 (6)	2.2	1.3	4.1
$\Delta H^{\neq}$ (kJ.mol^{-1})	28 (6)	49	52.4	49.8
τ_R^{298} (ps)	75 (2)	98	76	77
E_R (kJ.mol^{-1})	9.1.10^{-2}	17	28	16.1

[a] From ref.[43]. [b] From ref [46]; [c] From ref.[70]

The water exchange rate of GdL3H is 4.8.10^6 s^{-1}, which is higher than that of GdL1 or GdL2.[43] Interestingly, it is in the same order of magnitude than that of GdDOTA, but higher than that of GdDO3APyNH$_2$. In the case of dissociative exchange for all DTPA- and DOTA-derivatives, it was generally observed that the replacement of one negatively charged carboxylate in the complex with a neutral amide decreases the exchange rate to about one third.[71] The same phenomenon was observed with GdDO3APyNH$_2$, for which a neutral pyridinic ligand replaces a carboxylate.[46] The higher water exchange rate observed for GdL3H can be explained by the steric crowding around the Gd^{3+} due to the bulky imidazothiadiazole heterocycle compared to the pyridine. This is in line with previous results demonstrating an acceleration of the water exchange rate with the steric crowding.[65] Moreover, the presence of several other heteroatom nearby the water molecule can also accelerate the water exchange rate through hydrogen bonding networks.

The rotational correlation time is 75 ps, which is similar to that of GdDOTA, and slightly lower than that of GdL1 or GdL2, in accordance with the smaller size of the complex, and explaining the slightly lower relaxivity.

The pH-dependence of the relaxivity was also investigated at 60 MHz, 25°C in the pH range 3.8 – 12. The results, presented in Figure 8, show that the relaxivity is constant in the pH-range studied. The first protonation step of the complex (Log *K* = 9.0) was not expected to alter the relaxivity as it occurs on the nitrogen atom of the thiazole ring of the heterocycle, but interestingly the second protonation step (Log *K* = 4.5) is not influencing the relaxivity either. This second protonation step was expected to happen either on the nitrogen of the imidazole moiety or on a carboxylate function in the vicinity of the heterocycle. When the nitrogen atom of the imidazole moiety protonates, the heterocycle dissociates from the Ln^{3+}, and it is clear, from DFT calculations, that the Ln^{3+} would be bishydrated in this environment, leading to a substantial increase of the relaxivity below pH 6 (see species distribution in Figure 8). This is not the case, which means that the second protonation should occur on the carboxylate function, while keeping a monohydrated complex as previously observed in the solid state and solution properties of such LnDOTA derivatives.[48]

 This journal is © The Royal Society of Chemistry 2024

Please do not adjust margins

Please do not adjust margins

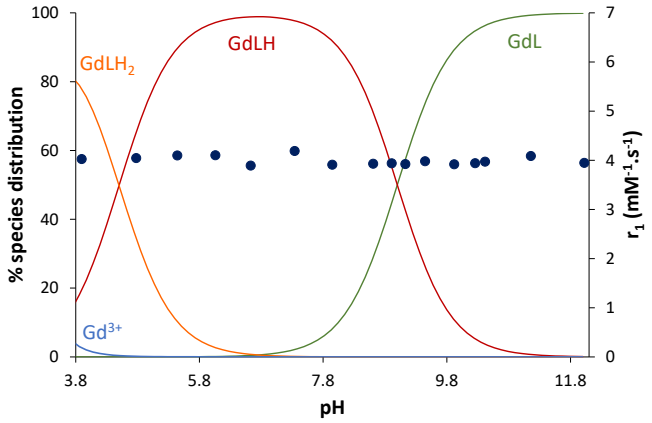

Figure 8: pH-dependency of the relaxivity of GdL3H at 60 MHz, 25°C, together with the species distribution calculated from data in Tables 1 and 3.

Conclusions

In conclusion, we have developed an efficient synthetic pathway to DO3A ligands substituted with an imidazothiadiazole scaffold for Ln^{3+} complexation. The potentiometric studies of the resulting systems show the formation of a stable Gd^{3+} complex with two protonation constants. These protonation steps could be attributed to the nitrogen atom located on the thiazole moiety of the heterocycle and to a carboxylate function in the vicinity of the heterocycle. The protonation of the latter is stabilized by the formation of H-bond with the heterocycle. This results in a slightly lower stability constant value of the Gd^{3+} complex compared to other Gd^{3+} DO3A complexes with a direct coordination of a pyridinic moiety. The selectivity of the ligand for Gd^{3+} vs Zn^{2+} is ensured by the very good kinetic inertness of the system. The kinetic inertness of the system had to be determined in highly acidic media as the complex is very inert in modest acidic conditions, and in the presence of competing metal ions, demonstrating the strong inertness of the system. A full characterization of the solution structure of the Ln^{3+} complex was undertaken by a combination of DFT calculations and NMR experiments (^{1}H, ^{13}C and ^{89}Y) on the paramagnetic Eu^{3+} and diamagnetic Y^{3+} complexes. The well-resolved Eu^{3+} ^{1}H NMR spectrum evidenced the presence of two isomers (SAP and TSAP) of C1 symmetry, with a slightly favoured TSAP isomer compared to GdDOTA. The coordination of the heterocycle to the Ln^{3+} was demonstrated by DFT calculations and supported by the experimental ^{89}Y chemical shift, which evidenced a N_5O_4 coordination sphere of the Ln^{3+} with one coordinated water molecule, as also evidenced by luminescence lifetimes measurements on the Tb^{3+} complex. Photophysical studies show the sensitization of Tb^{3+} luminescence by the imidazothiadiazole moiety with relative modest quantum yield values, that are nevertheless at least ten times higher than those of TbL1 and TbL2 due to the direct coordination of the heterocycle. The presence of the coordinated water molecule allows for achieving relaxivities higher than that of GdDOTA and consistent with the size of the system. Interestingly the water exchange rate, as assessed by ^{17}O NMR is similar to that of GdDOTA due to a combination of a less negative and more crowded environment around Gd^{3+}. The relaxivity is constant over the whole range of studied pH. Compared to the previous generation of complexes, for which the heterocycle was linked to the macrocycle through an amide function, the direct substitution on the macrocycle allows for the coordination of the heterocycle to the Ln^{3+}. This leads to optimized quantum yield for the Tb^{3+} complex, and water exchange rate for the Gd^{3+} complex. Importantly the resulting Ln^{3+} complexes are thermodynamically stable and kinetically inert. The presence of protonated complex is observed and can be explained by H-bonding network with the heterocycle. The tuning of the position of the heteroatoms within the heterocycle should allow to tune the presence of these protonated species and further optimize the kinetic inertness of the system. All together, this coordination study of Ln^{3+} by an imidazothiazole moiety shows promise in terms of thermodynamic stability, kinetic inertness, photophysical and relaxation properties of the system, which should pave the route for the development of efficient systems optimized for imaging properties and with potential therapeutic applications.

Experimental part

General Information. ^{1}H NMR and ^{13}C NMR spectra were recorded on a Bruker DPX 400 MHz instrument using $CDCl_3$ and DMSO–d_6 or on a Bruker Advance III HD Spectrometer at 298 K using a 5 mm BBFO probe. ^{1}H and ^{13}C spectra were obtained respectively at 600 MHz and 150 MHz. The chemical shifts are reported in parts per million (δ scale), and all coupling constant (J) values are reported in hertz. The following abbreviations were used for the multiplicities: s (singlet), d (doublet), t (triplet), q (quartet), p (pentuplet), m (multiplet), sext (sextuplet), and dd (doublet of doublets). All compounds were characterized by ^{1}H NMR, and ^{13}C NMR which are consistent with those reported in the literature (Supplementary Materials). Melting points are uncorrected. IR absorption spectra were obtained on a PerkinElmer PARAGON 1000 PC, and the values are reported in inverse centimeters. High-resolution mass spectra (HRMS) were recorded on a Bruker Q-TOF MaXis spectrometer. The reactions were monitored by thin-layer chromatography (TLC) using aluminum (Kiesel gel 60F254, Merck, Darmstadt, Germany) and visualized using ultraviolet light (λ = 254 nm or 365 nm). Column chromatography was performed using silica gel 60 (0.063–0.200 mm, Merck). Microwave irradiation was carried out in sealed vessels placed in a Biotage Initiator or Biotage Initiator+ system (400 W maximum power). The temperatures were measured externally by IR. Pressure was measured by a non–invasive sensor integrated into the cavity lid. All reagents were purchased from commercial suppliers and were used without further purification.

Synthesis and characterization

Ethyl 2-methylimidazo[2,1-*b*][1,3,4]thiadiazole-6-carboxylate 2. 2-amino-5-methyl-1,3,4-thiadiazole **1** (0.5 g, 4.34 mmol, 1 eq.) and ethyl bromopyruvate (1 mL, 7.96 mmol, 1.8 eq.) are dissolved in 15

Please do not adjust margins

Please do not adjust margins

mL of ethanol and stirred under microwave activation during 1.5 h at 100 °C. Then, the solvent is evaporated under reduced pressure and 20 mL of sodium bicarbonate is added to the resulting oil. The solution is extracted three times with 20 mL of DCM and the combined organic phases are washed with 20 mL of brine, dried over $MgSO_4$ and concentrated under reduce pressure. The crude product is purified by flash chromatography with the following eluent (AcOEt/PE 70/30), to yield compound **2** as a yellow solid (275 mg, 30%). Spectral data correspond to literature.

(2-methylimidazo[2,1-*b*][1,3,4]thiadiazol-6-yl)methanol 3. Compound **2** (383 mg, 1.81 mmol, 1.0 eq.) is dissolved under inert atmosphere at 0°C in 20 mL of anhydrous DCM. Then, DIBAL-H (1M in toluene) (8.16 mL, 8.16 mmol, 4.5 eq.) is added dropwise and the mixture is stirred at room temperature during 24 h. The mixture is diluted with 10 mL of a saturated Rochelle's salt solution and stirred during 24 h. The solution is extracted twice with 10 mL of DCM, then twice with 10 mL of EtOAc. The organic phases are collected, dried over $MgSO_4$ and evaporated under reduced pressure. The compound **3** is obtained (272 mg, 89%) as a light-yellow solid. Mp = 111-113 °C.; ^{1}H RMN (400 MHz, DMSO-d_6) δ (ppm): 6.94 (s, 1H), 4.20 (t, *J* = 5.7Hz, 1H), 3.51 (d, *J* = 5.6Hz, 2H), 1.77 (s, 3H).; ^{13}C NMR (101 MHz, DMSO-d_6) δ (ppm): 159.9, 147,4, 143.9, 111.0, 58.2, 17.4; HRMS (EI-MS) m/z calcd for $C_6H_8N_3OS$: 170.0386 $[M+H]^+$, found: 170.0383.

6-(Chloromethyl)-2-methylimidazo[2,1-*b*][1,3,4]thiadiazole 4. A solution of **3** (0.154 mg, 0.91 mmol, 1.0 eq.) is prepared in 5 mL of dry DCM. The solution is cooled at 0 °C and $SOCl_2$ (0.1 mL, 1.4 mmol, 1.5 eq.) is added dropwise. The mixture is stirred at 0 °C during 1 h and then, stirred at room temperature overnight. 10 mL of water are added to quench the reaction. Next, 10 mL of DCM were added and the solution is neutralized in order to reach pH 7-8 with a solution of saturated $NaHCO_3$. Aqueous phase was extracted twice with 10 mL DCM, and the combined organic phases are washed with 10 mL of brine, then dried over $MgSO_4$, filtrated and concentrated under reduced pressure. The product is purified by flash chromatography with the following eluent (PE/EtOAc 70/30). The compound **4** is obtained (101 mg, 59%) as a beige solid. Mp = 101-103 °C.; ^{1}H NMR (400 MHz, $CDCl_3$) δ (ppm): 7.70 (s, 1H), 4.64 (s, 2H), 2.69 (s, 3H).; ^{13}C NMR (101 MHz, $CDCl_3$) δ (ppm): 160.1, 145.6, 142.4, 112.2, 39.9, 17.8; HRMS (EI-MS) m/z calcd for $C_6H_7ClN_3S$: 188.0045 $[M+H]^+$, found: 188.0043.

2,2',2''-(10-((2-Methylimidazo[2,1-*b*][1,3,4]thiadiazol-6-yl)methyl)-1,4,7,10-tetraazacyclododecane-1,4,7-triyl)triacetic acid L3. Compound **4** (150 mg, 0.80 mmol, 1.0 eq.) and potassium carbonate (792mg, 5.7 mmol, 7.0 eq.) is added to a 15 mL solution of ^{t}BuODO$_3$A (617 mg, 1.2 mmol, 1.5 eq.) in anhydrous acetonitrile. The mixture is heated at 50 °C and stirred during 24 h. Then, potassium carbonate is filtered and washed twice with 10 mL of DCM. The solvent is evaporated under reduced pressure. The resulting yellow oil is dissolved in 5 mL of dioxane and a 5mL solution of hydrochloric acid (HCl 10 M) is added. The mixture is stirred during 16 h at 50 °C. After that, the solvents are evaporated under reduced pressure, and the crude product is dissolved in a 2 mL of MilliQ to adjust its pH between 4-5 with a aq. 2 M NaOH solution. Finally, the crude product is purified by flash chromatography on reversed phase with a gradient MilliQ water/MeOH (100:0 / 50:50 / 0:100). The resulting product **L3** is isolated (98 mg, 25%) as a white solid. ^{1}H NMR (600 MHz, D_2O) δ (ppm): 8.02 (s, 1H), 3.96 (s, 2H), 3.82 - 2.96 (m, 25H), 2.71 (s, 3H).; ^{13}C NMR (151 MHz, D_2O) δ (ppm): 163.8, 145.8, 115.1, 56.1, 55.0-49.5, 48.7, 48.0, 16.8; HRMS (EI-MS) m/z calcd for $C_{20}H_{31}N_7O_6S$: 498.2131 $[M+H]^+$, found: 498.2129.

Liquid sample preparation. The ligand concentrations were determined by adding an excess of zinc solution to a ligand solution and titrating the metal excess with standardized Na_2H_2EDTA in urotropine buffer (pH 5.6–5.8) in the presence of Xylenol Orange or Eriochrome Black T, or Murexide as indicators. The concentration of the metal solutions were determined similarly by complexometric titrations. The complexes were prepared by mixing 1 eq. of L, with 1 eq. of Ln^{3+}, and the pH was adjusted to 7.4 either with a buffered solution or by adding KOH or HCl to the solution. The absence of free Ln^{3+} was checked by the Xylenol orange test. The concentrations of Ln^{3+}-containing solutions were also checked both by ICP-OES and BMS measurements when possible.

GdL3: HRMS (EI-MS) m/z calcd for $C_{20}H_{31}N_7O_6SGd$: 653.1136 $[M+H]^+$, found: 653.1133.

EuL3: ^{1}H NMR (700 MHz, D_2O): see Figure S14. HRMS (EI-MS) m/z calcd for $C_{20}H_{31}N_7O_6SEu$: 648.1107 $[M+H]^+$, found: 648.1111.

YL3: ^{1}H NMR (600 MHz, D_2O): see Figure S16. HRMS (EI-MS) m/z calcd for $C_{20}H_{31}N_7O_6SY$: 584.0953 $[M+H]^+$, found: 584.0953.

TbL3: HRMS (EI-MS) m/z calcd for $C_{20}H_{31}N_7O_6STb$: 654.1148 $[M+H]^+$, found: 654.1144.

Potentiometric Studies. Carbonate-free 0.1 M NaOH and 0.1 M HCl were prepared from Fisher Chemicals concentrates. Potentiometric titrations were performed in 0.15 mol. L^{-1} aqueous NaCl under nitrogen atmosphere and the temperature was controlled to 25.0±0.1 °C with a circulating water bath. The p[H] (p[H] = -log[H^+], concentration in molarity) was measured in each titration with a combined pH glass electrode (Metrohm) filled with 3M KCl and the titrant addition was automated by use of a 702 SM titrino system (Metrohm). The electrode was calibrated in hydrogen ion concentration by titration of HCl with NaOH in 0.15 M electrolyte solution.[72] A plot of meter reading versus p[H] allows the determination of the electrode standard potential (E°) and the slope factor (f). Continuous potentiometric titrations with HCl and NaOH 0.1 M were conducted on aqueous solutions containing 5 mL of L in NaCl 0.15 M, with 2 minutes waiting between successive points. The titrations of the metal complexes (Ca^{2+}, Zn^{2+}) were performed with the same ligand solutions containing 1 equivalent of metal cation, with 2 minutes waiting time between 2 points. To determine the stability constant of GdL3, the out-of-cell batch method was used: 24 batch samples were prepared between pH 2 and 6 at 1:1 Gd/L ratio (1.3 mM in NaCl 0.15 M). The samples were kept at 25°C for 1 week, until the equilibrium was reached. Experimental data was refined using the computer program Hyperquad 2008.[73] All equilibrium

 This journal is © The Royal Society of Chemistry 2024

Please do not adjust margins

Please do not adjust margins

constants are concentration quotients rather than activities and are defined as:

$$K_{mhl} = \frac{[M_m L_l H_h]}{[M]^m [L]^l [H]^h}$$

The ionic product of water at 25 °C and 0.15 molL^{-1} ionic strength is pKw = 13.77.[74] Fixed values were used for pKw, ligand acidity constants and total concentrations of metal, ligand and acid. All values and errors (one standard deviation) reported are at least the average of three independent experiments.

Photophysical measurements. For the determination of the protonation constants, samples of L3 and GdL3 0.15 mM, were titrated with NaOH or HCl in NaCl 0.1 M. , UV-visible absorption spectra were recorded at 298 K on a Perkin Elmer UV/Vis/NIR Spectrometer Lambda 19 in the range λ = 200-500 nm with data steps of 1 nm, with a 1 cm path length. Luminescence measurements were performed at 298 K on an Agilent Cary Eclipse Fluorescence spectrophotometer with an emission filter 295-1100nm, slit widths 5 nm for excitation and emission wavelengths. The data was treated with HypSpec.[73, 75] For photophysical measurements with Tb^{3+} complexes, 0.5 mM solutions in HEPES buffer (pH=7.4, 100 mM) or D_2O (pD = 7.4) were prepared. For collecting photophysical data, samples were placed into 2.4 mm i.d. quartz capillaries or quartz Suprasil cells (Hellma® 115F-QS, bandpass 0.2 or 1 cm). Absorption spectra were measured on a Jasco V-670 UV/Visible/NIR spectrophotometer. Emission and excitation spectra were measured on a Horiba-Jobin-Yvon Fluorolog 3 spectrofluorimeter. All spectra were corrected for the instrumental functions. Luminescence lifetimes were determined under excitation at 266 nm provided by a YG 980 Quantel Nd:YAG laser while the Tb^{3+} signal was selected using an iHR320 monochromator (Horiba Scientific) and detected using a R928 photomultiplier tube (185-900 nm). The output signal from the detector was then fed to a Tektronix TDS 754C 500MHz bandpass digital oscilloscope and then transferred to a PC for treatment with Origin 9®. Luminescence lifetimes are averages of at least three independent measurements. Tb^{3+}-centered quantum yields were determined with a Fluorolog 3 spectrofluorimeter using an integration sphere (Model G8, GMP SA, Renens, Switzerland) and 0.1 mM solution of TbL_1 complex from Ref. [20] as a standard (Q_{Tb}^L = 37±1% in HEPES buffer, pH 7.4). Estimated experimental error for quantum yields determination is 10 %.

NMR experiments

The NMR spectra of EuL3H in D_2O (1.98 mM, pD = 6.97) were recorded at 298 K on a Bruker Avance III HD 700 equipped with a CPTCI cryoprobe. When necessary a solvent suppresion was achieved using an excitation sculpting sequence or a presaturation pulse. ^{1}H, ^{13}C COSY and HSQC were recorded. The NMR spectra of YL3H in D_2O (4.60 mM, pD = 7.36) were recorded at 298 K on a Bruker Advance III HD Spectrometer at 298 K using a 5 mm BBFO probe and at 600 MHz for the ^{1}H. ^{1}H, ^{13}C COSY, HMBC and HMQC were recorded. The ^{89}Y chemical shifts were obtained using a ^{1}H-^{89}Y HMQC experiment with a delay for evolution of long-range or couplings of 41.66 ms and a 2 s delay for relaxation time. ^{89}Y chemical shifts were expressed in ppm relative to Y(EDTA) as external reference.[61]

DFT calculations. Geometry optimizations were carried out with the Gaussian 16 program package (revision C.01),[76] using either the hybrid, long-range corrected wB97XD[77] density functional, which includes atom–atom dispersion corrections, or the hybrid-meta GGA functional TPSSh.[78] The inner electrons of Gd (46+4f^7) were treated with a large-core quasirelativistic effective core potential, employing a [5s4p3d]-GTO basis set for outermost 11 electrons.[79] For yttrium we selected the effective core potential ECP28MDF [80](28 electrons in the core) and its associated VTZ basis set. All other atoms were described using the Def2-TZVPP basis set[81]. The effects of bulk water were incorporated in all Gaussian calculations using the integral equation formalism of the polarized continuum model (IEFPCM).[82] The ^{89}Y NMR shielding tensors were calculated with the GIAO[83, 84] method and the TPSSh functional, using the ORCA program package (Version 5.0.4) [85, 86] and the ZORA[87] relativistic method. In these calculations we used the zora-def2-TZVPP basis set for ligand atoms, which contains the exponents of the def2-TZVPP basis set and was recontracted for ZORA calculations by D. A. Pantazis. For yttrium, we selected the SARC-ZORA-TZVPP[88] basis set. The resolution of identity and chain of spheres (RIJCOSX)[89-91] approximation was used to accelerate the SCF calculations and the calculation of nuclear magnetic resonance chemical shielding constants,[92] with the help of the SARC/J basis set for yttrium and the Def2/J[93] basis set for all other atoms. Bulk solvents were considered using the SMD solvation model.[94]

Relaxometric measurements. Proton NMRD profiles were recorded at 1.09 mM in Hepes buffer (0.1 M, pH 7.4) on a Stelar SMARTracer Fast Field Cycling relaxometer (0.01-10 MHz) and a Bruker WP80 NMR electromagnet adapted to variable field measurements (20-80 MHz) and controlled by a SMARTracer PC-NMR console. The temperature was monitored by a VTC91 temperature control unit and maintained by a gas flow. The temperature was determined by previous calibration with a Pt resistance temperature probe. The longitudinal relaxation rates ($1/T_1$) were determined in water.

Temperature dependent ^{17}O NMR measurements. The transverse and longitudinal ^{17}O NMR relaxation rates ($1/T_2$, $1/T_1$) and the chemical shifts were measured in aqueous solutions of [GdL3] = 1.8 mM in the temperature range 278-348 K, on a Bruker Avance 400 (9.4 T, 54.5 MHz) spectrometer. The temperature was calculated according to previous calibration with ethylene glycol and methanol.[95] An acidified water solution ($HClO_4$, pH 3.3) was used as external reference. Transverse relaxation times (T_2) were obtained by the Carr-Purcell-Meiboom-Gill spin-echo technique.[96] The technique of the ^{17}O NMR measurements on Gd^{3+} complexes has been described elsewhere.[97] The samples were sealed in glass spheres fitted into 10 mm NMR tubes to avoid susceptibility corrections of the chemical shifts.[98] To improve the sensitivity ^{17}O-enriched water (10 % $H_2{}^{17}O$, CortectNet) was added to reach around 1 % enrichment. The least-square fit of the ^{17}O NMR were performed using Visualiseur/Optimiseur[99] running on a MATLAB 8.3.0 (R2014a) platform.

Please do not adjust margins

Please do not adjust margins

Author Contributions

E. Caillet, L. Nunes, M. Ndiaye: Investigation and Vizualisation. S.V. Eliseeva: Investigation and writing -original draft. A. Pallier, M. Isaac and J-F. Morfin: Supervision, Writing-review and editing. H. Meudal: Investigation. S. Petoud and S. Routier: Supervision, Writing, review and editing. C. Platas-Iglesias: Conceptualization, Investigation, Writing – original draft. F. Buron, C.S. Bonnet: Conceptualization, Project Management, Funding Acquisition, Writing-original draft.

Conflicts of interest

There are no conflicts to declare.

Acknowledgements

Authors gratefully acknowledge the Région Centre Val de Loire (RTR Motivhealth), the Labex programs SYNORG (ANR-11-LABX-0029) and IRON (ANR-11-LABX-0018-01), the Ligue contre le Cancer du Grand Ouest (comités des Deux Sèvres, du Finistère, de l'Ile et Villaine, du Loir et Cher, de Loire Atlantique, du Loiret, de la Vienne, du Morbihan, de l'Eure et Loire), ITMO Cancer of Aviesan within the framework of the 2021-2030 cancer control strategy, on funds administrated by Inserm, and the Réseau 'Molécules Marines, Métabolisme & Cancer' of the Cancéropôle Grand Ouest for their financial support. This project has received funding from the European Union's Horizon 2020 research and innovation program under the Marie Sklodowska-Curie agreement No 898850. FB and SR thank the projects CHemBio (FEDER-FSE 2014-2020-EX003677), Valbiocosm (FEDER-FSE 2014-2020-EX003202), Techsab (FEDER-FSE 2014-2020-EX011313), QUALICHIM (APR-IA-PF 2021-00149467), for their financial support of ICOA, UMR 7311, University of Orléans, CNRS." We also thank the SALSA and MO2VING platforms for spectroscopic measurements spectrometric and chromatographic analyses (NMR, HPTLC, HPLC, MS, HRMS). C. P.-I. Thanks Centro de Supercomputación de Galicia (CESGA) for providing access to supercomputing facilities. S.P. acknowledges support from Institut National de la Santé et de la Recherche Médicale (INSERM).

Notes and references

1. J.-C. G. Bunzli, *Acc. Chem. Res.*, 2006, **39**, 53-61.
2. D. Parker, R. S. Dickins, H. Puschmann, C. Crossland and J. A. K. Howard, *Chem. Rev.*, 2001, **102**, 1977-2010.
3. A. E. Merbach, L. Helm and E. Toth, *The Chemistry of Contrast Agents in Medical Magnetic Resonance Imaging*, John Wiley & Sons, Chichester, Second Edition edn., 2013.
4. J. Wahsner, E. M. Gale, A. Rodríguez-Rodríguez and P. Caravan, *Chemical Reviews*, 2019, **119**, 957-1057.
5. S. V. Eliseeva and J.-C. G. Bunzli, *Chem. Soc. Rev.*, 2010, **39**, 189.
6. S. Sun, Y. Zhao, J. Wang and R. Pei, *J. Mater. Chem. B*, 2022, **10**, 9535-9564.
7. S. Lacerda, K. Djanashvili and C. S. Bonnet, in *Supramolecular Chemistry in Biomedical Imaging*, eds. S. Faulkner, T. Gunnlaugsson and G. O Maille, The Royal Society of Chemistry, 2022, DOI: 10.1039/9781782624028-00163, pp. 163-206.
8. C. Herlan and S. Bräse, *Dalton Trans.*, 2020, **49**, 2397-2402.
9. M. Van de Voorde, K. Van Hecke, T. Cardinaels and K. Binnemans, *Coord. Chem. Rev.*, 2019, **382**, 103-125.
10. N. S. Chundawat, S. Jadoun, P. Zarrintaj and N. P. S. Chauhan, *Polyhedron*, 2021, **207**, 115387.
11. J.-C. G. Bunzli, *Chem. Rev.*, 2010, **110**, 2729-2755.
12. E. Brucher, G. Tircso, Z. Baranayai, Z. Kovacs and A. D. Sherry, in *The Chemistry of Contrast Agents in Medical Magnetic Resonance Imaging*, eds. A. E. Merbach, L. Helm and E. Toth, John Woley & Sons, Chichester, Second Edition edn., 2013, ch. Four, pp. 157-208.
13. S. Shuvaev, M. Starck and D. Parker, *Chem. Eur. J.*, 2017, **23**, 9974-9989.
14. K. P. Malikidogo, H. Martin and C. S. Bonnet, *Pharmaceuticals*, 2020, **13**, 436.
15. J. Lux and A. D. Sherry, *Curr. Opin. Chem. Biol.*, 2018, **45**, 121-130.
16. A. D. Sherry, D. D. Castelli and S. Aime, *NMR in Biomedicine*, 2023, **36**, e4698.
17. S. Lacerda, *Inorganics*, 2018, **6**, 129.
18. P. Désogère, S. B. Montesi and P. Caravan, *Chem. Eur. J.*, 2019, **25**, 1128-1141.
19. E. Gianolio, R. Stefania, E. Di Gregorio and S. Aime, *Eur. J. Inorg. Chem.*, 2012, **2012**, 1934-1944.
20. J. He, C. S. Bonnet, S. V. Eliseeva, S. Lacerda, T. Chauvin, P. Retailleau, F. Szeremeta, B. Badet, S. Petoud, E. Toth and P. Durand, *J. Am. Chem. Soc.*, 2016, **138**, 2913-2916.
21. N. Hamon, L. Bridou, M. Roux, O. Maury, R. Tripier and M. Beyler, *J. Org. Chem.*, 2023, **88**, 8286-8299.
22. G. Nizou, C. Favaretto, F. Borgna, P. V. Grundler, N. Saffon-Merceron, C. Platas-Iglesias, O. Fougère, O. Rousseaux, N. P. van der Meulen, C. Müller, M. Beyler and R. Tripier, *Inorg. Chem.*, 2020, **59**, 11736-11748.
23. M. Le Fur, E. Molnár, M. Beyler, O. Fougère, D. Esteban-Gómez, O. Rousseaux, R. Tripier, G. Tircsó and C. Platas-Iglesias, *Inorg. Chem.*, 2018, **57**, 6932-6945.
24. C. P. Montgomery, B. S. Murray, E. J. New, R. Pal and D. Parker, *Acc. Chem. Res.*, 2009, **42**, 925-937.
25. L. M. T. Frija, A. J. L. Pombeiro and M. N. Kopylovich, *Coord. Chem. Rev.*, 2016, **308**, 32-55.
26. G. Mercuri, G. Giambastiani and A. Rossin, *Inorganics*, 2019, **7**, 144.
27. B. A. Bhongade, S. Talath, R. A. Gadad and A. K. Gadad, *J Saudi Chem. Soc.*, 2016, **20**, S463-S475.
28. H. A. Mohamed and B. F. Abdel-Wahab, *J. Sulfur Chem.*, 2012, **33**, 589-604.
29. S. Saba, in *Comprehensive Heterocyclic Chemistry II*, eds. A. R. Katritzky, C. W. Rees and E. F. V. Scriven, Pergamon, Oxford, 1996, DOI: https://doi.org/10.1016/B978-008096518-5.00173-8, pp. 191-198.
30. A. Cristina, D. Leonte, L. Vlase, L. C. Bencze, S. Imre, G. Marc, B. Apan, C. Mogoșan and V. Zaharia, *Journal*, 2018, **23**.
31. N. Terzioglu and A. Gürsoy, *Eur. J. Med. Chem.*, 2003, **38**, 781-786.
32. R. Romagnoli, P. G. Baraldi, F. Prencipe, J. Balzarini, S. Liekens and F. Estévez, *Eur. J. Med. Chem.*, 2015, **101**, 205-217.
33. W. S. Alwan, R. Karpoormath, M. B. Palkar, H. M. Patel, R. A. Rane, M. S. Shaikh, A. Kajee and K. P. Mlisana, *Eur. J. Med. Chem.*, 2015, **95**, 514-525.
34. J. Marco-Contelles, E. Pérez-Mayoral and P. Ballesteros, in *Comprehensive Heterocyclic Chemistry III*, eds. A. R.

 This journal is © The Royal Society of Chemistry 2024

Please do not adjust margins

Please do not adjust margins

Katritzky, C. A. Ramsden, E. F. V. Scriven and R. J. K. Taylor, Elsevier, Oxford, 2008, DOI: https://doi.org/10.1016/B978-008044992-0.01005-1, pp. 199-305.

35. H. M. Patel, B. Sing, V. Bhardwaj, M. Palkar, M. S. Shaikh, R. Rane, W. S. Alwan, A. K. Gadad, M. N. Noolvi and R. Karpoormath, *Eur. J. Med. Chem.*, 2015, **93**, 599-613.
36. S. Cascioferro, G. Li Petri, B. Parrino, B. El Hassouni, D. Carbone, V. Arizza, U. Perricone, A. Padova, N. Funel, G. J. Peters, G. Cirrincione, E. Giovannetti and P. Diana, *Molecules*, 2020, **25**, 329.
37. C. Pescheteau, M. Place, A. Sava, L. Nunes, L. Profire, S. Routier and F. Buron, *RSC Adv.*, 2022, **12**, 6303-6313.
38. M. Place, C. Copin, M. Apotrosoaei, S. Constantin, I. M. Vasincu, L. Profire, F. Buron and S. Routier, *J. Org. Chem.*, 2017, **82**, 13700-13707.
39. C. Copin, N. Henry, F. Buron and S. Routier, *Synlett*, 2016, **27**, 1091-1095.
40. C. Copin, F. Buron and S. Routier, *Eur. J. Org. Chem.*, 2016, **2016**, 1958-1962.
41. C. Copin, S. Massip, J.-M. Léger, C. Jarry, F. Buron and S. Routier, *Eur. J. Org. Chem.*, 2015, **2015**, 6932-6942.
42. C. Copin, N. Henry, F. Buron and S. Routier, *Eur. J. Org. Chem.*, 2012, **2012**, 3079-3083.
43. M. Ndiaye, E. Caillet, S. V. Eliseeva, T. Masson, L. A. Marchetti, A. Pallier, J.-F. Morfin, S. Petoud, S. Routier, F. Buron and C. S. Bonnet, *in revision*, 2023.
44. M. Regueiro-Figueroa, B. Bensenane, E. Ruscsák, D. Esteban-Gómez, L. J. Charbonnière, G. Tircsó, I. Tóth, A. d. Blas, T. Rodríguez-Blas and C. Platas-Iglesias, *Inorg. Chem.*, 2011, **50**, 4125-4141.
45. S. Laine, R. Jouclas, C. S. Bonnet, P. Retailleau, V. Steinmetz, A. Pallier, Z. Garda, G. Tircsó, P. Durand and É. Tóth, *Eur. J. Inorg. Chem.*, **n/a**, e202300784.
46. S. Laine, R. Jouclas, C. S. Bonnet, P. Retailleau, V. Steinmetz, A. Pallier, Z. Garda, G. Tircso, P. Durand and E. Toth, *Submitted*.
47. K. Kumar, C. A. Chang, L. C. Francesconi, D. D. Dischino, M. F. Malley, J. Z. Gougoutas and M. F. Tweedle, *Inorg. Chem.*, 1994, **33**, 3567-3575.
48. C. Harriswangler, J. C. Frías, M. T. Albelda, L. Valencia, E. García-España, D. Esteban-Gómez and C. Platas-Iglesias, *Inorg. Chem.*, 2023, **62**, 17030-17040.
49. J. A. K. Howard, A. M. Kenwright, J. M. Moloney, D. Parker, M. Woods, J. A. K. Howard, M. Port, M. Navet and O. Rousseau, *Chem. Commun.*, 1998, DOI: 10.1039/A802847H, 1381-1382.
50. M. Storm Thomsen, H. O. B. Andersen and T. J. Sørensen, *Dalton Trans.*, 2022, **51**, 14118-14124.
51. M. Regueiro-Figueroa, E. Ruscsák, L. Fra, G. Tircsó, I. Tóth, A. de Blas, T. Rodríguez-Blas, C. Platas-Iglesias and D. Esteban-Gómez, *Eur. J. Inorg. Chem.*, 2014, **2014**, 6165-6173.
52. S. Gündüz, S. Vibhute, R. Botár, F. K. Kálmán, I. Tóth, G. Tircsó, M. Regueiro-Figueroa, D. Esteban-Gómez, C. Platas-Iglesias and G. Angelovski, *Inorg. Chem.*, 2018, **57**, 5973-5986.
53. Z. Baranyai, Z. Pálinkás, F. Uggeri, A. Maiocchi, S. Aime and E. Brücher, *Chem. Eur. J.*, 2012, **18**, 16426-16435.
54. A. Takács, R. Napolitano, M. Purgel, A. C. Bényei, L. Zékány, E. Brücher, I. Tóth, Z. Baranyai and S. Aime, *Inorg. Chem.*, 2014, **53**, 2858-2872.
55. A. Rodríguez-Rodríguez, M. Regueiro-Figueroa, D. Esteban-Gómez, T. Rodríguez-Blas, V. Patinec, R. Tripier, G. Tircsó, F. Carniato, M. Botta and C. Platas-Iglesias, *Chem. Eur. J.*, 2017, **23**, 1110-1117.
56. Z. Garda, V. Nagy, A. Rodríguez-Rodríguez, R. Pujales-Paradela, V. Patinec, G. Angelovski, É. Tóth, F. K. Kálmán, D. Esteban-Gómez, R. Tripier, C. Platas-Iglesias and G. Tircsó, *Inorg. Chem.*, 2020, **59**, 8184-8195.
57. E. J. Corey and J. C. Bailar, Jr., *J. Am. Chem. Soc.*, 1959, **81**, 2620-2629.
58. J. K. Beattie, *Acc. Chem. Res.*, 1971, **4**, 253-259.
59. S. Aime, M. Botta and G. Ermondi, *Inorg. Chem.*, 1992, **31**, 4291-4299.
60. C. Platas-Iglesias, *Eur. J. Inorg. Chem.*, 2012, **2012**, 2023-2033.
61. Y. Xing, A. K. Jindal, M. Regueiro-Figueroa, M. Le Fur, N. Kervarec, P. Zhao, Z. Kovacs, L. Valencia, P. Pérez-Lourido, R. Tripier, D. Esteban-Gómez, C. Platas-Iglesias and A. D. Sherry, *Chem. Eur. J.*, 2016, **22**, 16657-16667.
62. J. C. Facelli, *Prog. Nucl. Magn. Reson. Spectrosc.*, 2011, **58**, 176-201.
63. J.-C. G. Bünzli, *Coord. Chem. Rev.*, 2015, **293-294**, 19-47.
64. A. Beeby, D. Parker and J. A. G. Williams, *J. Chem. Soc., Perkin Trans.*, 1996, 1565-1579.
65. E. Toth, L. Helm and A. E. Merbach, in *The Chemistry of Contrast Agents in Medical Magnetic Resonance Imaging*, eds. A. E. Merbach, L. Helm and E. Toth, John Wiley & Sons, Chichester, Second Edition edn., 2013, ch. 2, pp. 25-81.
66. P. H. Fries and E. Belorizky, *J. Chem. Phys.*, 2005, **123**, 124510.
67. P. Mieville, H. Jaccard, F. Reviriego, R. Tripier and L. Helm, *Dalton Trans.*, 2011, **40**, 4260.
68. P. Caravan, J. J. Ellison, T. J. McMurry and R. B. Lauffer, *Chem. Rev.*, 1999, **99**, 2293-2352.
69. B. Halle and H. Wennerstrom, *J. Chem. Phys.*, 1981, **75**, 1928-1943.
70. D. H. Powell, O. M. NiDhubhghaill, D. Pubanz, L. Helm, Y. S. Lebedev, W. Schlaepfer and A. E. Merbach, *J. Am. Chem. Soc.*, 1996, **118**, 9333-9346.
71. E. Toth, L. Helm and A. Merbach, in *The Chemistry of Contrast Agents in Medical Magnetic resonance Imaging*, eds. A. Merbach, L. Helm and E. Toth, John Wiley & Sons, Chichester, Second Edition edn., 2013, pp. 25-81.
72. A. E. Martell and R. J. Motekaitis, *Determination and use of stability constants*, VCH, 1992.
73. P. Gans, A. Sabatini and A. Vacca, *Talanta*, 1996, **43**, 1739-1753.
74. R. M. Smith, R. J. Motekaitis and A. E. Martell, NIST Standard Reference Database).
75. P. Gans, A. Sabatini and A. Vacca, *Ann. Chim. (Rome)*, 1999, **89**, 45-49.
76. M. J. Frisch, G. W. Trucks, H. B. Schlegel, G. E. Scuseria, M. A. Robb, J. R. Cheeseman, G. Scalmani, V. Barone, G. A. Petersson, H. Nakatsuji, X. Li, M. Caricato, A. V. Marenich, J. Bloino, B. G. Janesko, R. Gomperts, B. Mennucci, H. P. Hratchian, J. V. Ortiz, A. F. Izmaylov, J. L. Sonnenberg, Williams, F. Ding, F. Lipparini, F. Egidi, J. Goings, B. Peng, A. Petrone, T. Henderson, D. Ranasinghe, V. G. Zakrzewski, J. Gao, N. Rega, G. Zheng, W. Liang, M. Hada, M. Ehara, K. Toyota, R. Fukuda, J. Hasegawa, M. Ishida, T. Nakajima, Y. Honda, O. Kitao, H. Nakai, T. Vreven, K. Throssell, J. A. Montgomery Jr., J. E. Peralta, F. Ogliaro, M. J. Bearpark, J.

Please do not adjust margins

Please do not adjust margins

J. Heyd, E. N. Brothers, K. N. Kudin, V. N. Staroverov, T. A. Keith, R. Kobayashi, J. Normand, K. Raghavachari, A. P. Rendell, J. C. Burant, S. S. Iyengar, J. Tomasi, M. Cossi, J. M. Millam, M. Klene, C. Adamo, R. Cammi, J. W. Ochterski, R. L. Martin, K. Morokuma, O. Farkas, J. B. Foresman and D. J. Fox, *Journal*, 2016.
77. J.-D. Chai and M. Head-Gordon, *Phys. Chem. Chem. Phys.*, 2008, **10**, 6615-6620.
78. J. Tao, J. P. Perdew, V. N. Staroverov and G. E. Scuseria, *Phys. Rev. Lett.*, 2003, **91**, 146401.
79. M. Dolg, H. Stoll, A. Savin and H. Preuss, *Theor. Chim. Acta*, 1989, **75**, 173-194.
80. K. A. Peterson, D. Figgen, M. Dolg and H. Stoll, *J. Chem. Phys.*, 2007, **126**.
81. F. Weigend and R. Ahlrichs, *Phys. Chem. Chem. Phys.*, 2005, **7**, 3297-3305.
82. J. Tomasi, B. Mennucci and R. Cammi, *Chem. Rev.*, 2005, **105**, 2999-3094.
83. R. Ditchfield, *J. Chem. Phys.*, 2003, **56**, 5688-5691.
84. T. Helgaker, M. Jaszuński and K. Ruud, *Chem. Rev.*, 1999, **99**, 293-352.
85. F. Neese, *WIREs Computational Molecular Science*, 2012, **2**, 73-78.
86. F. Neese, *WIREs Computational Molecular Science*, 2018, **8**, e1327.
87. E. v. Lenthe, E. J. Baerends and J. G. Snijders, *J. Chem. Phys.*, 1993, **99**, 4597-4610.
88. J. D. Rolfes, F. Neese and D. A. Pantazis, *J. Comput. Chem.*, 2020, **41**, 1842-1849.
89. F. Neese, *J. Comput. Chem.*, 2003, **24**, 1740-1747.
90. S. Kossmann and F. Neese, *Chem. Phys. Lett.*, 2009, **481**, 240-243.
91. R. Izsák and F. Neese, *J. Chem. Phys.*, 2011, **135**.
92. G. L. Stoychev, A. A. Auer, R. Izsák and F. Neese, *J Chem Theory Comput*, 2018, **14**, 619-637.
93. F. Weigend, *Phys. Chem. Chem. Phys.*, 2006, **8**, 1057-1065.
94. A. V. Marenich, C. J. Cramer and D. G. Truhlar, *The Journal of Physical Chemistry B*, 2009, **113**, 6378-6396.
95. D. S. Raiford, C. L. Fisk and E. D. Becker, *Anal. Chem.*, 1979, **51**, 2050-2051.
96. S. Meiboom and D. Gill, *Review of Scientific Instruments*, 1958, **29**, 688-691.
97. K. Micskei, L. Helm, E. Brucher and A. E. Merbach, *Inorg. Chem.*, 1993, **32**, 3844-3850.
98. A. D. Hugi, L. Helm and A. E. Merbach, *Helv. Chim. Acta*, 1985, **68**, 508-521.
99. F. Yerly, *VISUALISEUR 2.3.5 and OPTIMISEUR 2.3.5*, Lausanne, Switzerland, 1999.

 This journal is © The Royal Society of Chemistry 2024

Please do not adjust margins